Combined use of wind-driven rain and wind pressure to define water penetration risk into building façades: the Spanish case

José M. Pérez-Bella[a], Javier Domínguez-Hernández[a,*], Beatriz Rodríguez-Soria[a], Juan J. del Coz-Díaz[b], Enrique Cano-Suñén[a]

[a] *Department of Construction Engineering, Engineering and Architecture School, University of Zaragoza, María de Luna, s/n, 50018, Zaragoza, Spain*

[b] *Department of Construction Engineering, University of Oviedo, Edificio Departamental Viesques nº 7, 33204 Gijón, Spain.*

Abstract

This article defines a new index to characterise the risk of atmospheric water penetration into building enclosures. This risk index integrates the two most relevant exposure parameters for this phenomenon into a single value, combining the water supply presented by driving rain and simultaneous wind pressure on the surface of the enclosure. Compared with the usual wind-driven rain exposure maps, the inclusion of driving rain wind pressure in this index permits a more complete assessment of the risk of penetration. Therefore, this index represents a powerful tool for defining more appropriate façade solutions for exposures that result in atmospheric water penetration. This risk index was calculated for 80 Spanish sites scattered around the Iberian Peninsula and the Canary and Balearic Islands using daily precipitation averages and wind speed averages for each location collected over 30 years. As a result, a risk index map has been produced for Spain. The risk characterisation obtained in this study enables an objective improvement of current Spanish building regulations governing the design of façades against the penetration of atmospheric water.

Keywords

Wind pressure, Wind-driven rain, Building design, Water tightness, Risk assessment, Spain

* Corresponding author. Department of Construction Engineering, University of Zaragoza, María de Luna, s/n, 50018, Zaragoza, Spain. Tel.Fax: +34 976 76 21 00.
E-mail address: javdom@unizar.es (Javier Domínguez-Hernández)

1. Introduction

Atmospheric precipitation accompanied by gusts of wind is the primary agent responsible for the wetting of building enclosures [1]. The action of wind pressure together with the effect of atmospheric precipitation allows water to penetrate the façades of buildings [2]. The wetting and penetration of water into enclosures reduces their durability [3, 4], decreases the ability of façades to insulate against increasing energy costs [5-7], and may affect the health of building occupants [8-10].

Although the penetration of the enclosure by water depends on complex mechanisms of moisture transport at a microscopic level [11-14], it essentially occurs as a result of the combined action of two atmospheric exposures: a sufficient intake of precipitation water (l/m^2) on the façade's vertical surface or wind-driven rain (*WDR*) and the action of wind pressure (Pa) simultaneous with precipitation or driving rain wind pressure (*DRWP*) [15].

Numerous studies have determined the characteristic *WDR* exposure in different countries [16-21], which has served as a starting point for defining performance-based enclosure designs to prevent moisture-related syndromes. Thereby each national regulation may determine façade designs that are appropriate at each location and operational condition, based on its wind-driven rain exposure [22]. However, this exposure does not consider the fundamental role of *DRWP* in the penetration of water [23] and therefore cannot individually characterise the risk of water penetration into façades. To the best of the authors' knowledge, few countries have complemented studies of *WDR* exposure by constructing maps of *DRWP* exposure [24].

This article defines a new index that characterises the overall risk of atmospheric water penetration and considers the combined action of both exposure parameters (*DRWP* and *WDR*) on building façades. This index can be used to develop risk maps in any country, thereby enabling the improvement of the design and performance of enclosures arranged in each location.

As an example, the water penetration risk map elaborated for Spain is presented, where current building regulations do not include the influence of any of the referred exposures for the proper design of façades [25]. For this purpose, daily weather data collected at 80 weather stations located at major airports and cities in Spain have been examined, and for the first time, a map of *DRWP* exposure for Spain has been developed.

The proposed risk index permits the joint quantification of the contribution of DRWP exposure, obtained in this study, and WDR exposure, identified by previous research [26], to atmospheric water penetration into enclosures throughout the entire Spanish mainland and its Balearic and Canarian archipelagos.

2. Background

To simulate real weather conditions that lead to the penetration of atmospheric water in enclosures, all standardised water tightness tests recreate both exposure parameters, i.e., pressure and water supply [27-32]. Thus, the test sample is subjected to varying conditions of pressure and water supply, simulating the *DRWP* and *WDR* exposures, respectively, that can occur simultaneously on the building enclosure. The characterisation of the water tightness is associated with the maximum pressure value supported during the test without presenting any water leakage on the inner surface of the façade sample. In all tests, the pressure difference applied is the driving parameter of the trial, using the water supply required to ensure the presence of a sheet of constant and uniform runoff water over the sample tested (ranging from 2 to 4 l/m^2min). Both parameters are different for each standarised test [33, 34].

The partial contribution of both exposure parameters in the process of penetration depends on the conditions of the enclosure [2]. Thus, in enclosures characterised by the absence of defects or pores larger than 1 mm (typical of new construction), the pressure difference across the façade (difference of indoor and outdoor wind pressure) is the most sensitive factor related to water penetration, regardless of the

existing water supply. However, in damaged enclosures, with defects, pores, or larger cracks (> 5 mm), water is able to penetrate the façade, even without high wind pressure.

Despite the importance of both atmospheric exposures in the process of water penetration, often only the value of wind-driven rain received in service conditions by the façades has been extensively characterised. Thus, different CFD and semi-empirical models have been developed in recent years to accurately determine this exposure [35-43]. However, the "WDR relationship" is more appropriate for rough approximations of the *WDR* exposure in large areas of a territory. This relationship (see Eq. 1) provides, by means of a coefficient *k* [44, 45], a semi-empirical relationship between the *WDR* received by the enclosure and the product of wind speed (U) and intensity of precipitation (R_h) recorded at each site [46, 47].

$$WDR = k \cdot U \cdot R_h \tag{1}$$

This general relationship or its variants, such as the ISO 15927-3:2009 [48], have been frequently used to elaborate national maps of exposure to driving rain [16-21]. However, *WDR* exposure alone is unable to characterise adequately the risk of water penetration into the enclosures of each site or region.

Thus, a high value of *WDR* may be due to conditions of intense precipitation R_h and low wind speed U (i.e., low wind pressure on the façade), which does not typically carry a high risk of water penetration in enclosures with good finishes, as are those commonly built and maintained as quality standards of developed countries. Therefore, an enclosure design based solely on the degree of *WDR* exposure would not be completely reliable.

To improve this situation, Section 3 presents a new risk index that assesses the combined influence of *DRWP* and *WDR* exposures at each site. Thus, both parameters are considered simultaneously, providing a more complete characterisation than an index based solely on the value of *WDR* exposure. The proposed risk index enables the identification of sites that are comparatively most likely to exhibit conditions for

water penetration in their enclosures and thus the creation of risk maps to improve the choice of façade systems suitable to the climatic conditions of each location.

To obtain this risk index, in addition to the *WDR* exposure values that are usually available at the sites of each country, the *DRWP* exposure in these same locations is needed. However, despite the importance of wind pressure in water penetration of façades, few studies have addressed this subject [2, 24]. The lack of values of *DRWP* in many countries hinders efforts to estimate accurately the pressure difference to be used to test water tightness in walls [15] and prevents a joint assessment of exposure conditions (*DRWP* and *WDR*) to which façades of buildings are subjected and which determine the overall risk of atmospheric water penetration [34].

Moreover, wind maps commonly used to characterise wind load on buildings are also not useful for defining the risk of water penetration into the façades, as they do not reflect the directional distribution or the intensity of wind pressure simultaneous with precipitation [49-51].

2.1 DRWP and WDR research conducted in Spain

Spain is no exception and lacks studies and maps on *DRWP* exposure. *WDR* exposure has recently been analysed in a large number of locations, thereby permitting the development of several maps of exposure [26].

Therefore, the current Spanish guidelines that establish façade building typologies for use in different locations to reduce the penetration risk of atmospheric water [25] have not been based on estimates of *DRWP* or *WDR*. Instead, the requirements imposed on the façades at each site are characterised on the basis of each of the areas as a result of combining a map of average annual rainfall and a map of basic wind speed (Fig. 1). These parameters are not temporally related (the basic wind speed is defined as the maximum wind speed that can occur over 10 minutes for a return period of 50 years), so they cannot

properly characterise the simultaneous amount of driving rain and wind pressure, nor do they permit an adequate characterisation of the risk of water penetration into the façades.

The need to jointly study *DRWP* and *WDR* exposure to improve this selection and design criteria for façade systems in Spain is reinforced by the varied rainfall, wind, and topography conditions of the Spanish sites. Thus, average rainfall of less than 300 mm/annum (in steppe or desert areas of the Canary Islands and the southeastern region of the Iberian Peninsula) to more than 2,000 mm/annum (on the country's Atlantic northern coast, even surpassing values of regions of northern Europe) are observed. In turn, Spain is in an area with low - to - moderate wind speeds; the basic wind velocity value (wind gust of 10 minutes and a 50-year return period) ranges, on average, between 26 and 29 m/s [52].

Figure 1. Average annual rainfall and basic wind velocity zones in Spain. Source: Spanish Technical Building Code [25].

The risk index defined in this article will improve this characterisation by developing a risk map of atmospheric water penetration for Spanish enclosures. First, the *DRWP* exposure at 80 Spanish sites will be determined from daily precipitation and wind speed data compiled by the Spanish Meteorological Agency (AEMET) for over 30 years at all sites. As a result, the article also presents the first map of *DRWP* exposure for Spain.

The risk index associated with each site is obtained by combining the *DRWP* exposure obtained at each site with the *WDR* exposure value identified in a previous study for the same locations [26]. The comparative analysis of the results of *DRWP* and *WDR* exposure obtained for the whole country, given the independence of both exposures, will reaffirm the need to include the effect of wind pressure simultaneous with precipitation to adequately characterise the risk of water penetration into façades.

The resulting risk map can be objectively used to improve the criteria used for choosing façade systems suitable to prevent problems associated with water penetration into buildings at each Spanish site.

3. Proposed risk index of water penetration in façades

A new normalised index (Risk Index of Water Penetration or *RIWP*), capable of integrating the two most relevant exposure parameters for water penetration in façades (*DRWP* and *WDR* exposure), is presented. To compare the risk of penetration at different locations, it is first necessary to normalise both exposure parameters with respect to the minimum and maximum values in the sample set. Equations 2 and 3 are proposed for this normalisation:

$$WDR_{normalized\ i} = \frac{WDR_i - WDR_{\min}}{WDR_{\max} - WDR_{\min}} \tag{2}$$

$$DRWP_{normalized\ i} = \frac{DRWP_i - DRWP_{\min}}{DRWP_{\max} - DRWP_{\min}} \tag{3}$$

The proposed normalisation, similar to those of other comparable nature indices [53], assigns the exposures at each of the locations a value of 0 to 1, representing the severity with respect to other sites in the sample space. The potential risk for water penetration enhances due to increases in the value of both normalised exposures.

To combine both normalised exposures into a single index, the Risk Index of Water Penetration (*RIWP*) for each site is obtained by Equation 4:

$$RIWP_i = \sqrt{\alpha \cdot \left(WDR_{normalized\ i}\right)^2 + \beta \cdot \left(DRWP_{normalized\ i}\right)^2} \tag{4}$$

To increase the applicability of this new index, two weighting factors (α and β) are included that permit the adaptation of the calculation of *RIWP* for its specific use in relation to certain types of façades. Thus,

the defined Risk Index of Water Penetration allows a risk assessment with a non-equivalent weighting of both parameters, increasing the partial influence of one of the exposures in water penetration.

Thus, for façades with defects, pores, and cracks of less than 1 mm (typically newly built or well-maintained), β can be larger than α, reflecting the greater influence of wind pressure in water penetration in this type of enclosure [2]. Conversely, to characterise specifically the risk of water penetration into damaged or poorly maintained façades, α should be greater than β, thus considering the major influence of the amount of water falling on the façade in the penetration process. This weighted characterisation can be applied to various fields of interest, such as the determination of areas for priority action in national programmes of façade rehabilitation. A specific value to α and β should not be provided without prior experimental tests conducted on similar walls.

The unique numerical value offered by the *RIWP* (associated with the risk of water penetration at each location) allows the definition of useful risk ranges for national regulations. Thus, for sites with risk in a specified range, façade solutions appropriate to that degree of risk may be prescribed in the same way that the *WDR* exposure maps are currently used in certain countries [22].

3.1 Exposure interval to consider

An important factor for calculating the risk of water penetration is the time interval of exposure, to which both parameters used (*DRWP* and *WDR*) are referenced. Usually, the process of water penetration into façades does not develop throughout the year but intensifies during short time intervals with a wetting stage on the façade, as defined in the standard ISO 15927-3 [48]. The standard includes the calculation of the *WDR* exposure associated with these wetting stages (time interval during which the supply of water due to rain is greater than the loss due to evaporation).

To estimate the wind-driven rain exposure in heavy masonry façades, this time interval (spell) is defined by the ISO standard as being limited by the occurrence of at least 96 hours devoid of wind-driven rain from a specific orientation, i.e., a different spell is defined over each orientation.

Therefore, the *DRWP* and *WDR* exposure values used in Eq. 2 and 3 for each possible direction of the façade should refer to this "spell" by means of the calculation process collected by the ISO 15927-3 standard.

4. Calculating RIWP in Spain

An example is shown below of the practical application of the Risk Index of Water Penetration in a particular region. As indicated previously, Spanish building regulations have not been based on *DRWP* or *WDR* values to define façade exposure to atmospheric water penetration; therefore, *RIWP* utilisation may constitute a significant advance.

To calculate this index in Spain, daily climate data sets provided by the Spanish Meteorological Agency (recorded at 80 stations spread across the country and representing different varieties of climate) were used. These data encompass more than 30 years of records, reaching 50 years (1962-2011) in 35 of the sites. The data include daily information about the value of precipitation, average wind speed, average temperature, and minimum and maximum range of atmospheric pressure.

4.1 DRWP analysis

The first exposure parameter required for the Risk Index of Water Penetration is the *DRWP* exposure associated with each location. For this parameter, climate data recorded during one day *i* with significant precipitation (> 0.05 mm) are used. Equation 5 defines the calculation of wind pressure value

simultaneous with driving rain *DRWP i* (Pa), where $\rho_{air\,i}$ (kg/m^3) represents the average density of the air during the day, and $U_{10\,i}$ (m/s) is the average value of wind speed recorded at a reference height of 10 m above ground level in a cleared area (airfield conditions):

$$DRWP_i = \frac{1}{2} \cdot \rho_{air\,i} \cdot U_{10\,i}^{\,2} \tag{5}$$

Air is considered an ideal gas, and its density $\rho_{air\,i}$ is determined according to Equation 6, where P_i is the absolute pressure (Pa) obtained as the average of the daily maximum and minimum recorded pressures ($P_{max\,i}$ and $P_{min\,i}$), T_i is the mean absolute temperature (K), and $R_{specific}$ is the specific gas constant for dry air (287.07 J/ kg K). To simplify the necessary calculation, the presence of air humidity has been neglected because no daily data for relative humidity are available for proper consideration. For those days for which one record (median temperature, high pressure, or low pressure) is missing, the air density is taken to be equal to 1.2 kg/m^3.

$$\rho_{air\,i} = \frac{P_i}{R_{specific} \cdot T_i} = \frac{0.5\left(P_{\max\,i} + P_{\min\,i}\right)}{287.07 \cdot T_i} \tag{6}$$

To establish the exposure interval under consideration, it is necessary to know that in Spanish buildings, there is a predominance of heavy masonry façades [54]; therefore, the value of *DRWP* exposure used to characterise the risk of penetration should refer to the exposure interval defined by the "spell" indicated by the ISO 15927-3 standard.

To determine the duration of each wetting stage or spell (limited by the occurrence of at least 96 hours devoid of wind-driven rain from a specific orientation), the ISO standard requires hourly and wind direction data that permit the referred calculation for each possible direction of the façade. However, in Spain, these hourly data are not sufficiently common, and available daily data do not provide information on wind direction. Thus, the method set by the ISO standard cannot be strictly applied to determine the

length of wetting stages, and a detailed analysis cannot be performed for each possible direction of the façade.

Instead, the length of an "absolute spell" can be determined as the number of days (*AS*) limited by the occurrence of four days (96 hours) devoid of wind-driven rain at the site (see Fig. 2). This adaptation of the spell concept [26] allows its calculation using daily data without information on wind direction, similar to the data available in Spain. Because the definition of this absolute spell does not consider wind direction relative to the orientation of the façade, any precipitation helps to prolong the period of the spell, regardless of wind direction.

Figure 2. "Absolute spell" proposed to evaluate the wetting stages of the enclosure using daily climatic data without information on wind direction (*No spell: at least 4 days without wind-driven rain at the site*).

To obtain the *DRWP* exposure value associated with each of the absolute spells that occur throughout each year, the average *DRWP* exposure during the *AS* days comprising each period can be considered. This $DRWP'_{AS}$ average value (Pa) is therefore defined by Equation 7:

$$DRWP'_{AS} = \frac{\sum_{i=1}^{AS} \frac{1}{2} \cdot \rho_{air\ i} \cdot U_{10\ i}{}^{2}}{AS} \quad (7)$$

To obtain a single reference value of exposure associated with wetting stages, the ISO standard sets the calculation of the maximum exposure value that may occur in one wetting stage with a return period of three years.

For this benchmark, a historical series that compiles obtained annual maximum values of $DRWP'_{AS}$ has been developed for each of the 80 sites analysed. Using this historical series and the Gumbel distribution,

the maximum $DRWP_{AS}$ expected in an absolute spell for a 3-year return period is determined. Table 1 shows a detailed example of this calculation conducted for one of the sites (Madrid airport).

Table 1. Calculation example of $DRWP_{AS}$ expected for a 3-year return period.

The results obtained by this method for the 80 sites examined are shown in Table 2. Based on these results, a map that represents the $DRWP_{AS}$ exposure in the Spanish sites was produced for the first time (Fig. 3). Because of the wide variety of climates [55] and topographies in the country, the value of $DRWP_{AS}$ varies widely from 11.31 Pa in Pontevedra (north-western coast) to 212.95 Pa in Izaña (mountain station in the Canary Islands).

Figure 3. $DRWP_{AS}$ associated with absolute spells and 3-year return period in Spain.

The largest exposure values are found in the Canary Islands, the Gulf of Cadiz, and the Strait of Gibraltar. The presence of particularly strong Atlantic winds in these regions justifies this increase in exposure. Meanwhile, the eastern and north-eastern regions of the country also exhibit significantly higher exposures than the central and northern regions of the peninsula, as a consequence of the particular climatic conditions of eastern Spain, where intense rainfall for short periods of time is common [56].

However, the northern coast of the country, which is characterised by longer wetting stages on the façade because of its high rainfall, shows much lower $DRWP_{AS}$ exposures, despite elevated exposure to Atlantic

winds. A greater number of days considered in the wetting stage decreases the average value of *DRWP* exposure and reduces the reference value associated with the wetting stage.

The resulting risk map can be compared with the current characterisation established by Spanish regulations. Comparing Figs. 1 and 3 reveals that the map of basic wind speed used (zones A, B, and C) does not identify the $DRWP_{AS}$ exposure with sufficient precision. The basic wind speed value assigned to each zone cannot be used to determine the value of this exposure either because the results that would be obtained by applying Eq. 5 (zone A, 405.6 Pa; zone B, 437.4 Pa; zone C, 504.6 Pa) are far superior to any of those shown in Fig 3.

Table 2. $DRWP_{AS}$ for 80 sites spread across the Spanish territory. Comparison with mean wind pressure and absolute spell wind-driven rain (WDR_{AS}).

This analysis of the $DRWP_{AS}$ exposure may be extended to a larger number of sites if suitable climatic data are available, thereby improving the coverage of the exposure map. To circumvent the usual lack of accurate weather data in many locations, we propose the use of average wind pressure for the site (which does not take into account the co-occurrence with precipitation) to approximate the value of $DRWP_{AS}$ exposure. To establish this approach, Table 2 also includes mean wind pressure values available for each location. As shown, the $DRWP_{AS}$ average value of the 80 sites analysed (40.93 Pa) is well above the average value of wind pressure (10.60 Pa); the calculation of the average value of wind pressure also includes days without precipitation and does not reflect the maximum value associated with a return period.

Fig. 4 shows the best possible linear fit between both magnitudes from the data obtained for the analysed sites (Izaña and the Navacerrada mountain pass are not representative of normal conditions in urban areas

and thus are not included in the linear adjustment and are not represented in the Fig 4). The low correlation coefficient obtained (R^2) is indicative of the limited accuracy of the established relationship. However, this simple adjustment can provide an approximate value of exposure for Spanish sites lacking simultaneous precipitation and wind data.

Figure 4. Best-fit linear relationship between $DRWP_{AS}$ and mean wind pressure in a daily interval.

4.2 WDR exposure data

The second of the exposure parameters required for the Risk Index of Water Penetration is the *WDR* exposure value associated with each location. Reference values of *WDR* exposure related to wetting stages have been obtained for a large number of sites in Spain [26].

The same guidelines previously presented were used for its calculation. Daily records of rainfall (R_h) and wind speed (U_{10}) were considered during the *AS* days that comprise each absolute spell. To obtain the WDR'_{AS} value associated with each of the absolute spells that occur throughout each year the ISO 15927-3:2009 formulation was used, eliminating its directional component (Eq. 8):

$$WDR'_{AS} = \frac{2}{9}\sum_{i=1}^{AS} U_{10\,i} \cdot \left(R_{h\,i}\right)^{8/9} \quad (8)$$

The reference exposure associated with these wetting stages (WDR_{AS}) was obtained as the maximum WDR'_{AS} expected in an absolute spell for a 3-year return period, in a similar way to Table 1 [26]. All these reference values are shown in Table 2 for the same 80 sites examined.

If the values of $DRWP_{AS}$ and WDR_{AS} obtained for these 80 Spanish sites are represented (Fig. 5), the independence between both exposure parameters can be observed. This independence, previously

identified by other studies [2], allows sites with low WDR_{AS} exposure (see Fig. 5) to exhibit a high $DRWP_{AS}$ exposure (i.e., a comparatively high risk of water penetration into the façade).

Figure 5. Convergence between WDR_{AS} and $DRWP_{AS}$ at 80 Spanish locations.

It is clear that the risk of atmospheric water penetration into the building enclosure should not be characterised by only one of the two exposure parameters involved in the process of penetration (*DRWP* or *WDR*). It would be necessary to integrate both exposures to characterise this risk adequately, as permitted by the proposed Risk Index of Water Penetration.

4.3 RIWP calculation

After obtaining the $DRWP_{AS}$ and WDR_{AS} reference values for each site in the sections above, the characteristic RIWP of each location and comparative risk of atmospheric water penetration at each site are determined. Both parameters are used to obtain normalised values of exposure parameters, as shown in Eqs. 2' and 3':

$$WDR_{AS\ normalized\ i} = \frac{WDR_{AS\ i} - WDR_{AS\min}}{WDR_{AS\max} - WDR_{AS\min}} \quad (2')$$

$$DRWP_{AS\ normalized\ i} = \frac{DRWP_{AS\ i} - DRWP_{AS\min}}{DRWP_{AS\max} - DRWP_{AS\min}} \quad (3')$$

The Risk Index of Water Penetration is calculated by combining both normalised exposures by Equation 4'. To generalise the applicability of the combined risk index obtained, a value that is equivalent and equal to 1 for the weighting factors α and β defined in Eq. 4 has been adopted:

$$RIWP_i = \sqrt{\left(WDR_{AS\ normalized\ i}\right)^2 + \left(DRWP_{AS\ normalized\ i}\right)^2} \quad (4')$$

The equivalent weight of both normalised parameters permits a general characterisation of the risk to enclosures with different surfaces and maintenance states, for which the relative influence of both exposures on water penetration can vary significantly [2]. The *RIWP* values obtained for the 80 analysed sites are collected in Table 3, along with the normalised values used for their determination.

Table 3. Risk Index of Water Penetration for 80 sites spread across the Spanish territory.

These data for the different Spanish sites are shown graphically, presenting for the first time a risk map for the entire country (Fig. 6). The risk index ranges from a value of 1.30 for Izaña Station (Canary Islands) to 0.07 for the city of Daroca (interior region of the country). The northern coast (despite its lower $DRWP_{AS}$ values), the Strait of Gibraltar, the Canary Islands, and the Gulf of Cadiz show a higher comparative risk of water penetration during wetting stages. In the interior region, significant risks are quantified only in the mountain sites, such as the Navacerrada mountain pass.

Figure 6. Risk Index of Water Penetration associated with absolute spells and 3-year return period in Spain.

The Proposed Risk Index of Water Penetration is the first comprehensive approach to characterising the risk of water penetration into façades and considers the climatic parameters most relevant to this phenomenon.

The simplifications introduced for its calculation in Spain (daily climate data usage versus hourly data) permit a rapid and simple application while enabling their use in a larger number of regions with climatic records of limited accuracy.

This index permits the comparison of the risk of water penetration between different sites, as well as the establishment of quantitative limits to prescribe enclosure solutions that are to be used in each of them. In this sense, Fig. 7 proposes a classification scheme based on the *RIWP* value that can supplement or replace the Spanish regulations presented above.

As limits to this classification, four ranges of risk associated with the value obtained are proposed: severe risk ($RIWP \geq 1.0$), high risk ($0.7 \leq RIWP < 1.0$), moderate risk ($0.4 \leq RIWP < 0.7$), and low risk ($RIWP < 0.4$). Each *RIWP* zone defines a group of sites having a similar potential of short-term water penetration. In this study, a *RIWP* value less than 0.4 has been considered to be associated with a comparatively low risk (65 of the 80 sites analysed in Spain would be associated with this group).

Figure 7. Viable classification scheme for locations based on the equivalence of both exposure parameters. *Only sites with radii that define a potential to present problems related to water penetration greater than 0.4 are shown.*

5. Conclusions

This paper presents a new index for the characterisation of the risk of penetration of atmospheric water in building enclosures by considering the characteristic values of wind-driven rain and driving rain wind pressure at each site. The index provides a tool of that will undoubtedly be useful for rigorously characterising the risk of penetration based on the most relevant atmospheric parameters involved in the

phenomenon. The index also opens a line of work focused on using this index in the field of enclosures with characteristic construction conditions, modifying the weighting factors included in its formulation.

The application of this index in Spain has allowed the development of a comprehensive risk map and the establishment of four different ranges of risk that can be used to supplement or replace the current Spanish regulation, improving the choice of appropriate façade solutions.

To calculate this risk index, a previous complete analysis of *DRWP* exposure conditions in the country was required, enabling the development for the first time of a map for this exposure parameter. A possible mathematical adjustment to estimate this exposure from the mean wind pressure available at any Spanish site has also been proposed. Finally, the analysis of the convergence between the values of *WDR* and *DRWP* exposure in Spain has empirically confirmed the need to consider both parameters to adequately characterise the risk of atmospheric water penetration.

As demonstrated by its application in Spain, the index presented may be applicable in any country, starting only with commonly available climate data. Therefore, this development can enhance and internationally complement the risk characterisation of water penetration based solely on wind-driven rain maps, helping to define façade construction solutions most appropriate to prevent problems related to this phenomenon.

Acknowledgments

These results were obtained from data provided by the Spanish Meteorological Agency, Ministry of Environment, Rural and Marine Affairs (AEMET). The authors wish to acknowledge the partial financial support provided by the Spanish Ministry of Science and Innovation through the Research Project BIA2012-31609 and the Research Project FICYT PC-10-33. We also recognise Javier Escuer Gracia for

his help in preparing the maps. Finally, the authors greatly appreciate the collaboration of the GICONSIME Research Group at the University of Oviedo.

References

[1] Blocken B, Carmeliet J. A review of wind-driven rain research in building science. J Wind Eng Ind Aerodyn 2004; 92 (13):1079–130. doi:10.1016/j.jweia.2004.06.003.

[2] Cornick SM, Lacasse MA. A review of climate loads relevant to assessing the watertightness performance of walls, windows, and wall-window interfaces. J ASTM Int 2005;2(10):1-16. doi:10.1520/JAI12505.

[3] Tang W, Davidson CI, Finger S, Vance K. Erosion of limestone building surfaces caused by wind-driven rain. 1. Field measurements. Atmos Environ 2004; 38(33): 5589-99. doi:10.1016/j.atmosenv.2004.06.030.

[4] Morrison Hershfield Limited. Survey of building envelope failures in the coastal climate of British Columbia. Ottawa: Canada Mortgage and Housing Corporation; 1996.

[5] Sanders C. Heat, air and moisture transfer in insulated envelope parts: Environmental conditions, vol 2. Leuven: International Energy Agency; 1996. Annex 24, Final report.

[6] del Coz JJ, García PJ, Díaz LM, Riesgo P. Nonlinear thermal analysis of multi-holed lightweight concrete blocks used in external and non-habitable floors by FEM. Int J Heat Mass Transfer 2011; 54(1–3): 533-548. doi: 10.1016/j.ijheatmasstransfer.2010.09.016.

[7] del Coz JJ, García PJ, Súarez JL, Rabanal FP, Lozano A, Domínguez J. Non-linear heat analysis of the performance of light concrete hollow brick walls by FEM. In: J.W. Bull editor. Computer Analysis and design of masonry structures. Saxe-Coburg Publications; 2012.

[8] Bornehag CG, Blomquist G, Gyntelberg F, Järvholm B, Malmberg P, Nordvall L, Nielsen A, Pershagen G, Sundell J. Dampness in buildings and health. Indoor Air 2001; 11: 72-86. doi: 10.1034/j.1600-0668.2001.110202.x.

[9] Haverinen-Shaughnessy U. Moisture as a source of indoor air contamination. EnVIE Conference on Indoor Air Quality and Health for EU Policy, Helsinki: 2007.

[10] WHO. Environmental burden of disease associated with inadequate housing. Methods for quantifying health impacts of selected housing risks in the WHO European Region. Copenhagen: World Health Organization; 2011.

[11] Rowell RL, Carrano SA, de Bethune AJ, Malinauskas AP. Gas and vapour permeability: Surface flow through porous media. J Colloid Interf Sci 1971; 37(1): 242-6. doi: 10.1016/0021-797(71)90286-4.

[12] Adolphs J, Setzer MJ. A model to describe adsorption isotherms. J Colloid Interf Sci 1996; 180 (1): 70-6. doi: 10.1006/jcis.1996.0274.

[13] Krus M. 1996. Moisture transport and storage coeffients of porous mineral building materials. Theoretical principles and new test methods. Stuttgart: Fraunhofer IRB Verlag; 1996.

[14] Franzen C, Mirwald PW. Moisture content of natural stone: static and dynamic equilibrium with atmospheric humidity. Environmental Geology 2004; 46: 391-401. doi: 10.1007/s00254-004-1040-1.

[15] Sahal AN, Lacasse MA. Experimental assessment of waterpenetration and entry into siding-clad wall specimen. National Research Council Canada; 2004. Internal Report No. 862. doi: irc_id:16429.

[16] Lacy RE. An Index of Exposure to Driving Rain. Garston: Building Research Establishment; 1971. Building Research Station, Digest No. 127.

[17] Boyd, DW. Driving rain map of Canada. Ottawa: National Research Council Canada; 1963. Technical note no. 398.

[18] Sauer P. An annual driving rain index for China. Building Environ 1987; 22:239-40. doi:10.1016/0360-1323(87)90016-3.

[19] Chand I, Bhargava PK. Estimation of driving rain index for India. Building Environ 2002; 37: 549-54. doi:10.1016/S0360-1323(01)00057-9.

[20] Sahal N. Proposed approach for defining climate regions for Turkey based on annual driving rain index and heating degree-days for building envelope design. Building Environ 2006; 41: 520-6. doi:10.1016/j.buildenv.2005.07.004.

[21] Giarma C, Aravantinos D. Estimation of building components' exposure to moisture in Greece based on wind, rainfall and other climatic data. J Wind Eng Ind Aerodyn 2011; 99: 91-102. doi:10.1016/j.jweia.2010.12.001.

[22] Office of the Deputy Prime Minister. The Building Regulations 2000. Approved Document C. C2 Resistance to the moisture. London; 2004.

[23] Lacasse MA, O'Connor T, Nunes SC, Beaulieu P. Report from Task 6 of MEWS Project: Experimental assessment of water penetration and entry into wood-frame wall specimens – Final Report. National Research Council Canada; 2003. doi: irc_id:15275.

[24] Welsh RE, Skinner WR, Morris RJ. A climatology of driving rain pressure for Canada. Climate and Atmospheric Research Directorate Draft Report, Environment Canada, Atmospheric Environment Service; 1989.

[25] Spanish Ministry of Housing. Spanish Building Technical Code. Basic Document HS1, Resistance to moisture. Madrid: 2006.

[26] Pérez JM, Domínguez J, Rodríguez B, del Coz JJ, Cano E. Estimation of the exposure to moisture in Spain from daily wind and rain data. Building Environ 2012; 57: 259-70. doi:10.1016/j.buildenv.2012.05.010.

[27] EN 12155. Curtain walling. Watertightness. Laboratory test under static pressure. European Committee for Standardization, 2000.

[28] EN 12865. Hygrothermal performance of building components and building elements. Determination of the resistance of external wall systems to driving rain under pulsating air pressure. European Committee for Standardization, 2001.

[29] AAMA 501.1-05. Standard test method for water penetration of exterior windows, curtain walls and doors using dynamic pressure. American Architectural Manufacturers Association, 2005.

[30] AS/NZS 4284. Testing of building Façades. Australian and New Zealand Standards Institution, 2008.

[31] ASTM E331-00. Standard test method for water penetration of exterior windows, skylights, doors, and curtain walls by uniform static air pressure difference. American Society for Testing and Materials, 2009.

[32] ASTM E547-00. Standard test method for water penetration of exterior windows, skylights, doors, and curtain walls by cyclic static air pressure difference. American Society for Testing and Materials, 2009.

[33] Sahal N, Lacasse MA. Proposed method for calculating water penetration test parameters of wall assemblies as applied to Istanbul, Turkey. Building and Environment 2008; 43: 1250-60. doi:10.1016/j.buildenv.2007.03.009

[34] Pérez JM, Domínguez J, Rodríguez B, del Coz JJ, Cano E. A new method for determining the water tightness of building façades. Building Research & Information 2013. doi:10.1080/09613218.2013.774936.

[35] Choi ECC. Numerical simulation of wind-driven-rain falling onto a 2-D building. In: Proceedings of Asia Pacific Conference on Computational Mechanics, Hong Kong: 1991, p. 1721-8.

[36] Choi ECC. Simulation of wind-driven rain around a building. J Wind Eng Ind Aerodyn 1993; 46&47: 721-9. doi: 10.1016/0167-6105(93)90342-L.

[37] Choi ECC. Determination of wind driven-rain intensity on building faces. J Wind Eng Ind Aerodyn 1994; 51(1):55-69. doi: 10.1016/0167-6105(94)90077-9.

[38] Choi ECC. Parameters affecting the intensity of wind-driven rain on the front face of a building. J Wind Eng Ind Aerodyn 1994; 53(1-2):1-17. doi: 10.1016/0167-6105(94)90015-9.

[39] Blocken B, Carmeliet J. Spatial and temporal distribution of driving rain on a low-rise building. Wind Struct 2002; 5(5):441-62.

[40] Straube JF, Burnett EFP. Simplified Prediction of Driving Rain Deposition. In: Proc. of International Building Physics Conference, Eindhoven: 2000, p. 375-82.

[41] Blocken B, Deszö G, van Beeck J, Carmeliet J. Comparison of calculation models for wind-driven rain deposition on building facades. Atmos Environ 2010; 44(14):1714-1725. doi:10.1016/j.atmosenv.2010.02.011.

[42] Blocken B, Abuku M, Nore K, Briggen P.M, Schellen H.L, Thue J.V, Roels S, Carmeliet J. Intercomparison of wind-driven rain deposition models based on two case studies with full-scale measurements. J Wind Eng Ind Aerodyn 2011; 99(4): 448–459. doi:10.1016/j.jweia.2010.11.004.

[43] Blocken B, Carmeliet J. Overview of three state-of-the-art wind-driven rain assessment models and comparison based on model theory. Building Environ 2010; 45(3):691-703. doi:10.1016/j.buildenv.2009.08.007.

[44] Lacy RE. Climate and Building in Britain. Her Majesty's Stationery Office 1977; London.

[45] Henriques FMA. Quantification of wind-driven rain. An experimental approach. A general review on driven rain and details of an experiment in Portugal to supplement existing research results in Norway, the UK and elsewhere. Building Research & Information 1992; 20 (5): 295-97. doi: 10.1080/09613219208727227.

[46] Hoppestad S. Slagregn i Norge (Driving rain in Norway, in Norwegian). Oslo: NBI; 1955. Norwegian Building Research Institute Report no. 13.

[47] Lacy RE, Shellard HC. An index of driving rain. Meteorological Mag 1962; 91(1080):177-84.

[48] EN ISO 15927-3. Hygrothermal performance of buildings — Calculation and presentation of climatic data Part 3: Calculation of a driving rain index for vertical surfaces from hourly wind and rain data. European Committee for Standardization; 2009.

[49] CMHC. Wind-Rain Relationships in Southwestern British Columbia. Ottawa: Canada Mortgage and Housing Corporation; 2007. Research Highlights, Technical Series 07-114.

[50] Kerr D. Keeping walls dry. Ottawa: Canada Montage and Housing Corporation; 2004.

[51] Pérez JM. Parameterization of moisture exposure and water tightness tests on external wall systems. Performance-based characterization of its hygrothermal behavior (in Spanish). Ph.D. Thesis. Construction Engineering Department, University of Zaragoza, Zaragoza, Spain, 2012. 960 p.

[52] EN 1991-1-4. Eurocode 1: Actions on structures - Part 1-4: General actions - Wind actions. European Committee for Standardization, 2005.

[53] Cornick S, Dalgliesh WA. A moisture index to characterize climates for building envelope desing. J Therm Envelope Build Sci 2003; 27(2): 151-178. doi:10.1177/109719603036210.

[54] Spanish Ministry of Public Works. Statistical information of Buildings. http://www.fomento.gob.es/mfom/lang_castellano/Estadisticas_y_Publicaciones/Informacion_Estadistica/Construccion/ConstruccionEdificios/Lmo_Publicacion/default.htm. [Accessed 25.10. 2012]

[55] Kottek M, Grieser J, Beck C, Rudolf B, Rubel F. World Map of the Köppen-Geiger climate classification updated. Meteorol. Z. 2006; 15:259-63. doi: 10.1127/0941-2948/2006/0130.

[56] Llasat MC, Martín F, Barrera A. From the concept of ‘‘Kaltlufttropfen’’ (cold air pool) to the cut-off low. The case of September 1971 in Spain as an example of their role in heavy rainfalls. Meteorol Atmos Phys 2007; 96: 43–60. doi: 10.1007/s00703-006-0220-9.

List of tables

Table 1.

Calculation example of $DRWP_{AS}$ expected for a 3-year return period.

Madrid airport. Station 3129. 40º28'00"N 03º33'20"W			
Year	Maximum value of yearly DRWP'$_{AS}$ (Pa)	Year	Maximum value of yearly DRWP'$_{AS}$ (Pa)
1962	89.32	1987	29.19
1963	59.15	1988	21.11
1964	30.62	1989	75.32
1965	58.63	1990	18.35
1966	23.50	1991	32.52
1967	27.18	1992	27.73
1968	40.07	1993	36.69
1969	27.70	1994	42.32
1970	17.76	1995	19.36
1971	19.01	1996	33.04
1972	19.84	1997	34.43
1973	19.00	1998	22.01
1974	25.31	1999	39.78
1975	26.44	2000	31.97
1976	33.99	2001	20.09
1977	35.47	2002	15.50
1978	49.35	2003	29.00
1979	22.85	2004	21.92
1980	32.59	2005	18.72
1981	35.31	2006	25.03
1982	56.46	2007	33.05
1983	36.90	2008	32.40
1984	34.33	2009	31.91
1985	90.55	2010	43.64
1986	29.32	2011	58.69

Magnitude	Value	Comment
N	50	Number of x_I data.
$\bar{x}$	34.688	Data average: $\bar{x} = \sum x_i / N$
σ_x	16.764	Standard deviation: $\sigma_x = \sqrt{\sum (x_i - \bar{x})^2 / N}$
u_y	0.549	Data average of 1 to N y_i values (reduced variable): $y_i = -\ln(\ln(N+1/i))$ *(Only depends on N value and could be approximated by a constant value of 0,5772)*
σ_y	1.161	Standard deviation of 1 to N y_i values (reduced variable): $y_i = -\ln(\ln(N+1/i))$ *(Only depends on N value and could be approximated by a constant value of 1,2856)*
u	36.765	Mode: $u = \bar{x} - u_y \frac{\sigma_x}{\sigma_y}$
α	0.069235	Dispersion parameter: $\alpha = \frac{\sigma_y}{\sigma_x} = \frac{1}{\beta}$

Cumulative distribution function. $F(x;\alpha;u) = \exp^{-\exp^{-y}} = \exp^{-\exp^{-\alpha(x-u)}}$

Return period	3 years	Taken in similarity to the ISO standard
1 – F(x;u;α)	0.3333	Probability of exceeding the x value.
x value	**39.804**	$DRWP_{AS}$ value (maximum $DRWP'_{AS}$ likely to occur once every 3 years in Pa).

Table 2.

$DRWP_{AS}$ for 80 sites spread across the Spanish territory. Comparison with mean wind pressure and absolute spell wind-driven rain (WDR_{AS}).

LOCATION	ALT. (m)	LATITUDE (DMS)	LONGITUDE (DMS)	$DRWP_{AS}$ (Pa)	Mean wind pressure (Pa)	WDR_{AS} [26] (mm)
La Coruña airport	98	43º18'25"N	08º22'20"W	29.52	10.63	364.71
La Coruña	58	43º22'02"N	08º25'10"W	29.48	11.00	296.14
Santiago airport	370	42º53'16"N	08º24'39"W	35.72	11.92	728.83
Vitoria airport	513	42º52'55"N	02º44'06"W	20.81	5.91	127.82
Albacete (Los Llanos)	704	38º57'08"N	01º51'47"W	74.64	14.98	75.88
Alicante airport	43	38º16'58"N	00º34'15"W	41.03	10.72	62.65
Alicante	81	38º22'21"N	00º29'39"W	19.47	4.20	44.78
Almería airport	21	36º50'47"N	02º21'25"W	69.69	15.24	59.62
Asturias airport	127	43º34'01"N	06º02'39"W	26.52	9.23	274.18
Oviedo	336	43º21'16"N	05º52'22"W	26.35	7.04	185.93
Ávila	1130	40º39'33"N	04º40'48"W	22.82	5.60	77.65
Badajoz airport	185	38º53'00"N	06º49'45"W	30.81	7.60	118.33
Barcelona airport	4	41º17'34"N	02º04'12"E	35.31	11.26	132.00
Burgos (Villafría)	890	42º21'22"N	03º37'57"W	46.86	14.09	182.13
Cáceres	405	39º28'20"N	06º20'22"W	32.93	7.85	166.30
Cádiz	1	36º30'04"N	06º15'24"W	63.30	13.63	228.35
Jerez airport	27	36º45'02"N	06º03'21"W	50.06	12.08	241.47
Tarifa	32	36º00'55"N	05º35'51"W	142.90	57.18	396.08
Santander airport	5	43º25'45"N	03º49'53"W	40.70	12.84	344.05
Santander	52	43º29'30"N	03º47'59"W	33.76	11.75	316.13
Castellón de la Plana	35	39º57'00"N	00º04'17"W	25.95	5.26	77.41
Ciudad Real	628	38º59'22"N	03º55'11"W	19.82	4.32	70.86
Córdoba airport	90	37º50'39"N	04º50'46"W	33.83	6.69	168.75
Cuenca	945	40º04'00"N	02º08'17"W	20.05	3.86	67.36
Gerona airport	143	41º54'42"N	02º45'48"E	19.50	5.33	87.67
Granada airport	567	37º11'23"N	03º47'22"W	18.37	4.22	56.08
Granada air base	687	37º08'13"N	03º37'53"W	25.47	5.47	67.50
Molina de Aragón	1056	40º50'40"N	01º53'07"W	25.89	4.41	63.15
San Sebastián airport	4	43º21'25"N	01º47'32"W	17.43	5.94	308.80
San Sebastián (Igueldo)	251	43º18'27"N	02º02'22"W	53.43	17.68	475.94
Huelva	19	37º16'48"N	06º54'35"W	30.11	8.66	135.86
Huesca airport	541	42º05'00"N	00º19'35"W	72.20	14.81	88.15
Ibiza airport	6	38º52'35"N	01º23'04"E	50.12	11.22	89.68
Menorca airport	91	39º51'17"N	04º12'56"E	57.42	15.02	142.41
Palma de Mallorca airport	8	39º33'39"N	02º44'12"E	44.54	9.77	80.06
Palma de Mallorca port	3	39º33'12"N	02º37'31"E	18.99	3.22	49.95
Jaén	582	37º46'40"N	03º48'27"W	20.26	3.60	102.10
Logroño airport	353	42º27'08"N	02º19'52"W	37.96	9.30	59.72
Fuerteventura airport	25	28º26'41"N	13º51'47"W	49.49	24.45	57.48
Lanzarote airport	14	28º57'07"N	13º36'01"W	48.76	27.84	61.71
Las Palmas de G. C. airport	24	27º55'21"N	15º23'22"W	78.40	13.17	63.97
León airport	916	42º35'20"N	05º38'58"W	35.91	7.64	100.26
Ponferrada	534	42º33'50"N	06º36'00"W	14.80	3.65	78.13
Lérida	192	41º37'33"N	00º35'42"E	19.18	5.19	36.20
Madrid airport	609	40º28'00"N	03º33'20"W	39.80	7.46	74.65
Madrid (Cuatro Vientos)	687	40º22'40"N	03º47'21"W	32.37	6.66	87.73
Madrid (Getafe)	617	40º18'00"N	03º43'21"W	45.75	9.13	85.91
Madrid	667	40º24'43"N	03º40'41"W	24.63	4.79	66.29
Madrid (Torrejón)	611	40º29'00"N	03º27'01"W	28.41	6.79	64.82
Navacerrada mountain pass	1894	40º46'50"N	04º00'37"W	32.83	7.66	459.94
Málaga airport	7	36º40'00"N	04º29'17"W	31.06	11.37	133.99
Melilla	47	35º16'40"N	02º57'19"W	51.38	12.17	108.35
Murcia (Alcantarilla)	85	37º57'28"N	01º13'47"W	20.53	4.84	39.95
San Javier airport	4	37º47'20"N	00º48'12"W	61.97	12.55	109.86
Pamplona airport	459	42º46'37"N	01º39'00"W	36.23	10.48	117.26
Pontevedra	108	42º26'24"N	08º36'59"W	11.31	3.65	286.68
Vigo airport	261	42º14'22"N	08º37'26"W	19.20	8.30	503.81
Salamanca airport	790	40º57'34"N	05º29'54"W	51.84	10.00	99.71
Salamanca	775	40º57'23"N	05º39'41"W	26.11	4.27	78.81

Segovia	1005	40º56’52”N	04º07’38”W	24.99	4.39	72.80
Morón de la Frontera	87	37º09’30”N	05º36’57”W	48.01	10.59	203.11
Sevilla airport	34	37º25’00”N	05º52’45”W	30.94	8.00	179.42
Soria	1082	41º46’30”N	02º28’59”W	38.75	7.59	94.21
Hierro airport	32	27º49’08”N	17º53’20”W	69.69	27.42	98.87
Izaña	2371	28º18’32”N	16º29’58”W	212.95	28.91	608.23
La Palma airport	33	28º37’59”N	17º45’18”W	94.90	19.56	176.99
Sta. Cruz de Tenerife	35	28º27’48”N	16º15’19”W	27.68	6.16	62.69
North Tenerife airport	632	28º28’39”N	16º19’46”W	56.38	18.89	206.18
South Tenerife airport	64	28º02’51”N	16º33’39”W	52.59	25.88	66.12
Reus airport	71	41º08’59”N	01º10’44”E	52.47	11.42	81.12
Tortosa	44	40º49’14”N	00º29’29”E	29.75	7.67	65.40
Toledo	515	39º53’05”N	04º02’58”W	29.45	5.92	58.97
Valencia airport	69	39º29’12”N	00º28’24”W	63.49	11.47	96.62
Valencia	11	39º28’50”N	00º21’59”W	21.04	3.69	71.49
Valladolid (Villanubla)	846	41º42’00”N	04º51’00”W	48.47	12.02	128.84
Valladolid	735	41º39’00”N	04º46’00”W	21.11	4.95	68.26
Bilbao airport	42	43º17’53”N	02º54’21”W	33.53	9.94	271.20
Zamora	656	41º31’00”N	05º44’01”W	18.81	4.44	69.97
Daroca	779	41º06’53”N	01º24’39”W	13.14	2.58	27.44
Zaragoza airport	247	41º39’43”N	01º00’29”W	62.59	20.58	52.83
Average results				40.93	10.60	

Table 3.

Risk Index of Water Penetration for 80 sites spread across the Spanish territory.

LOCATION	WDR_{AS} normalized	$DRWP_{AS}$ normalized	RIWP
La Coruña airport	0.50	0.14	0.52
La Coruña	0.41	0.14	0.43
Santiago airport	1.00	0.17	1.01
Vitoria airport	0.18	0.10	0.20
Albacete (Los Llanos)	0.10	0.35	0.37
Alicante airport	0.09	0.19	0.21
Alicante	0.06	0.09	0.11
Almería airport	0.08	0.33	0.34
Asturias airport	0.38	0.12	0.40
Oviedo	0.26	0.12	0.28
Ávila	0.11	0.11	0.15
Badajoz airport	0.16	0.14	0.22
Barcelona airport	0.18	0.17	0.25
Burgos (Villafría)	0.25	0.22	0.33
Cáceres	0.23	0.15	0.28
Cádiz	0.31	0.30	0.43
Jerez airport	0.33	0.24	0.41
Tarifa	0.54	0.67	0.86
Santander airport	0.47	0.19	0.51
Santander	0.43	0.16	0.46
Castellón de la Plana	0.11	0.12	0.16
Ciudad Real	0.10	0.09	0.13
Córdoba airport	0.23	0.16	0.28
Cuenca	0.09	0.09	0.13
Gerona airport	0.12	0.09	0.15
Granada airport	0.08	0.09	0.12
Granada air base	0.09	0.12	0.15
Molina de Aragón	0.09	0.12	0.15
San Sebastián airport	0.42	0.08	0.43
San Sebastián (Igueldo)	0.65	0.25	0.70
Huelva	0.19	0.14	0.23
Huesca airport	0.12	0.34	0.36
Ibiza airport	0.12	0.24	0.27
Menorca airport	0.20	0.27	0.33
Palma de Mallorca airport	0.11	0.21	0.24
Palma de Mallorca port	0.07	0.09	0.11
Jaén	0.14	0.10	0.17
Logroño airport	0.08	0.18	0.20
Fuerteventura airport	0.08	0.23	0.25
Lanzarote airport	0.08	0.23	0.24
Las Palmas de G. C. airport	0.09	0.37	0.38
León airport	0.14	0.17	0.22
Ponferrada	0.11	0.07	0.13
Lérida	0.05	0.09	0.10
Madrid airport	0.10	0.19	0.21
Madrid (Cuatro Vientos)	0.12	0.15	0.19
Madrid (Getafe)	0.12	0.21	0.25
Madrid	0.09	0.12	0.15
Madrid (Torrejón)	0.09	0.13	0.16
Navacerrada mountain pass	0.63	0.15	0.65
Málaga airport	0.18	0.15	0.23
Melilla	0.15	0.24	0.28
Murcia (Alcantarilla)	0.05	0.10	0.11
San Javier airport	0.15	0.29	0.33
Pamplona airport	0.16	0.17	0.23
Pontevedra	0.39	0.05	0.40
Vigo airport	0.69	0.09	0.70
Salamanca airport	0.14	0.24	0.28
Salamanca	0.11	0.12	0.16
Segovia	0.10	0.12	0.15

Morón de la Frontera	0.28	0.23	0.36
Sevilla airport	0.25	0.15	0.29
Soria	0.13	0.18	0.22
Hierro airport	0.14	0.33	0.35
Izaña	0.83	1.00	1.30
La Palma airport	0.24	0.45	0.51
Sta. Cruz de Tenerife	0.09	0.13	0.16
North Tenerife airport	0.28	0.26	0.39
South Tenerife airport	0.09	0.25	0.26
Reus airport	0.11	0.25	0.27
Tortosa	0.09	0.14	0.17
Toledo	0.08	0.14	0.16
Valencia airport	0.13	0.30	0.33
Valencia	0.10	0.10	0.14
Valladolid (Villanubla)	0.18	0.23	0.29
Valladolid	0.09	0.10	0.14
Bilbao airport	0.37	0.16	0.40
Zamora	0.10	0.09	0.13
Daroca	0.04	0.06	0.07
Zaragoza airport	0.07	0.29	0.30

Figure captions

Fig. 1. Average annual rainfall and basic wind velocity zones in Spain. Source: Spanish Technical Building Code [25].

Fig. 2. "Absolute spell" proposed to evaluate the wetting stages of the enclosure using daily climatic data without information on wind direction (*No spell: at least 4 days without wind-driven rain at the site*).

Fig. 3. $DRWP_{AS}$ associated with absolute spells and 3-year return period in Spain.

Fig. 4. Best-fit linear relationship between $DRWP_{AS}$ and mean wind pressure in a daily interval.

Fig. 5. Convergence between WDR_{AS} and $DRWP_{AS}$ in 80 Spanish locations.

Fig. 6. Risk Index of Water Penetration associated with absolute spells and 3-year return period in Spain.

Fig. 7. Viable classification scheme for locations based on the equivalence of both exposure parameters. *Only sites with radii that define a potential to present problems related to water penetration greater than 0.4 are shown.*

Figure 1

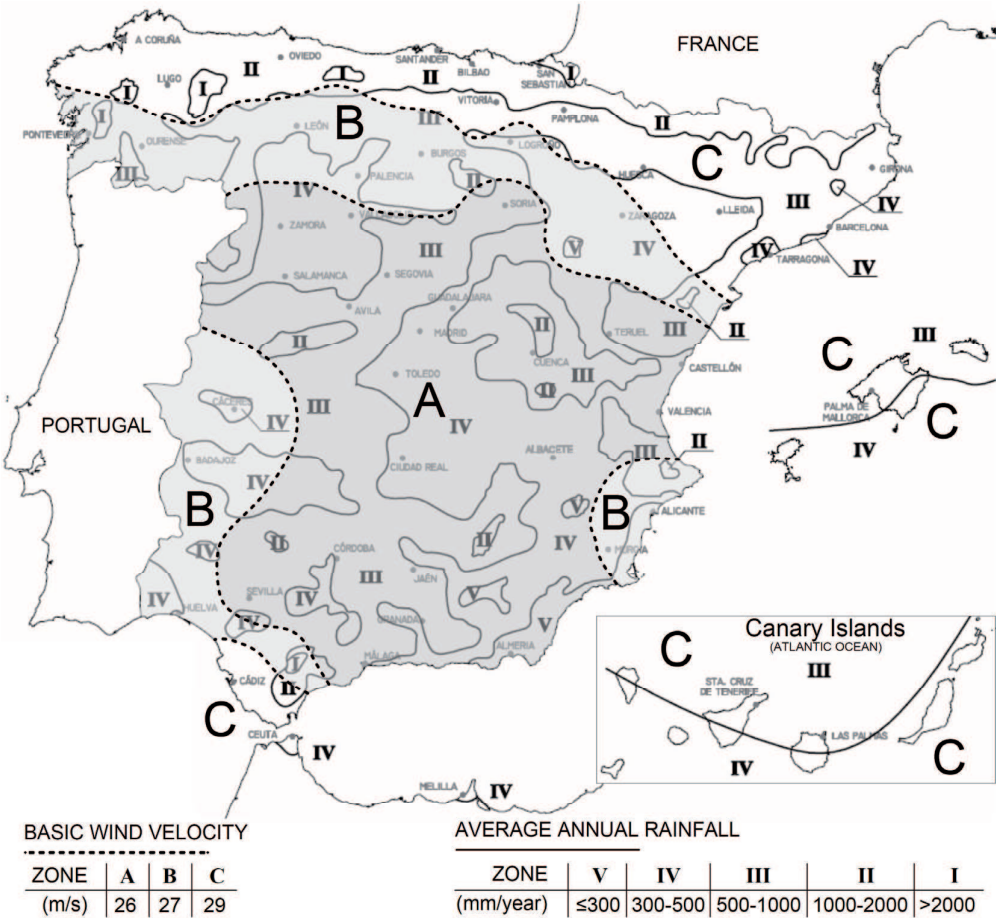

ZONE	A	B	C
(m/s)	26	27	29

ZONE	V	IV	III	II	I
(mm/year)	≤300	300-500	500-1000	1000-2000	>2000

Fig. 1. Average annual rainfall and basic wind velocity zones in Spain. Source: Spanish Technical Building Code [25].

Figure 2

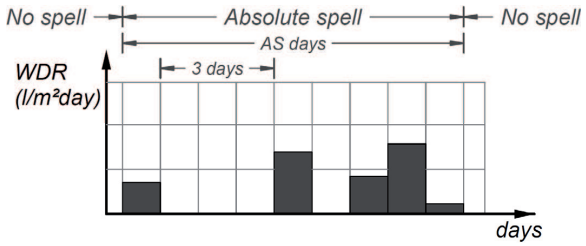

Fig. 2. "Absolute spell" proposed to evaluate the wetting stages of the enclosure using daily climatic data without information on wind direction (*No spell: at least 4 days without wind-driven rain at the site*).

Figure 3

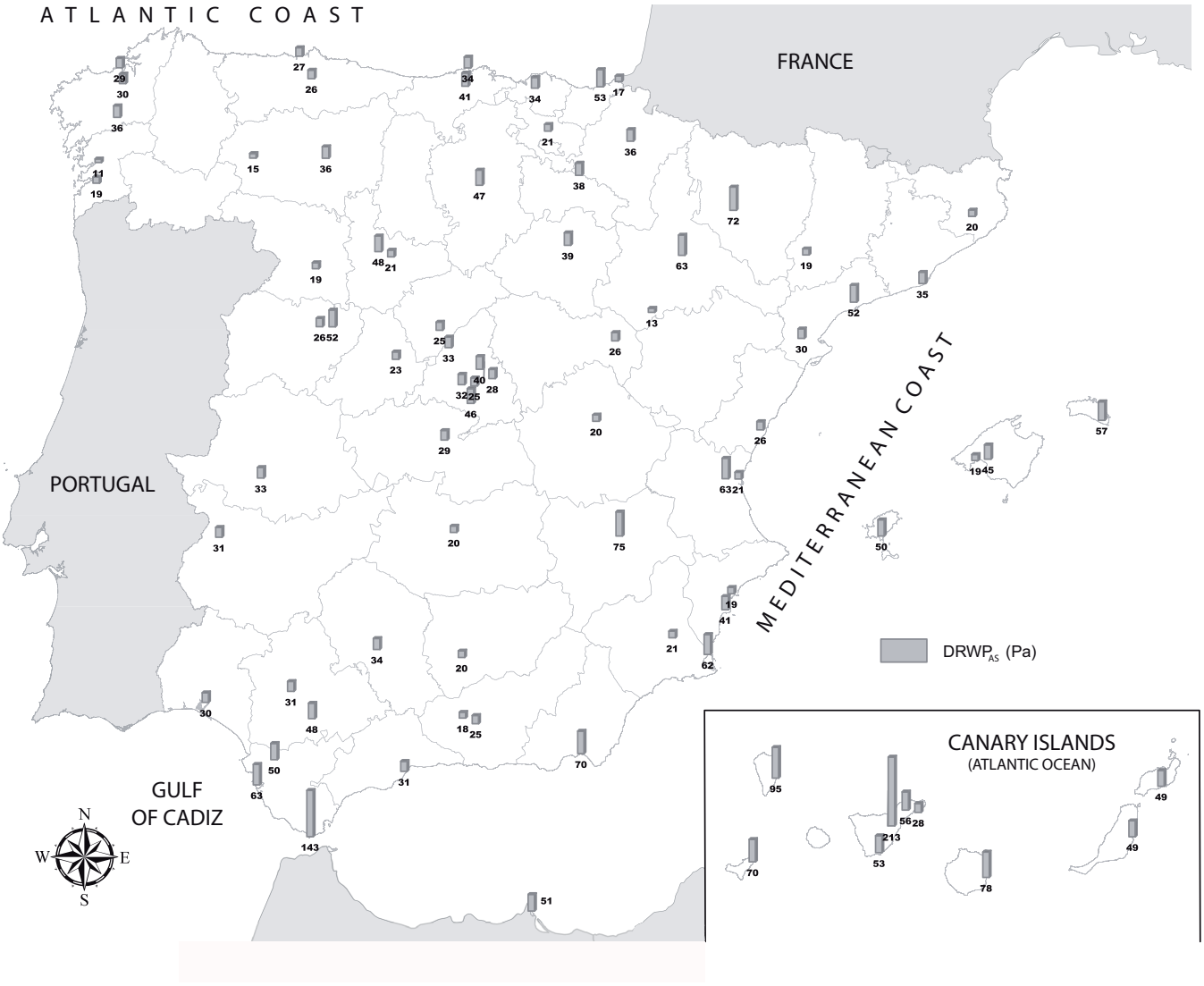

Fig. 3. $DRWP_{AS}$ associated with absolute spells and 3-year return period in Spain.

Figure 4

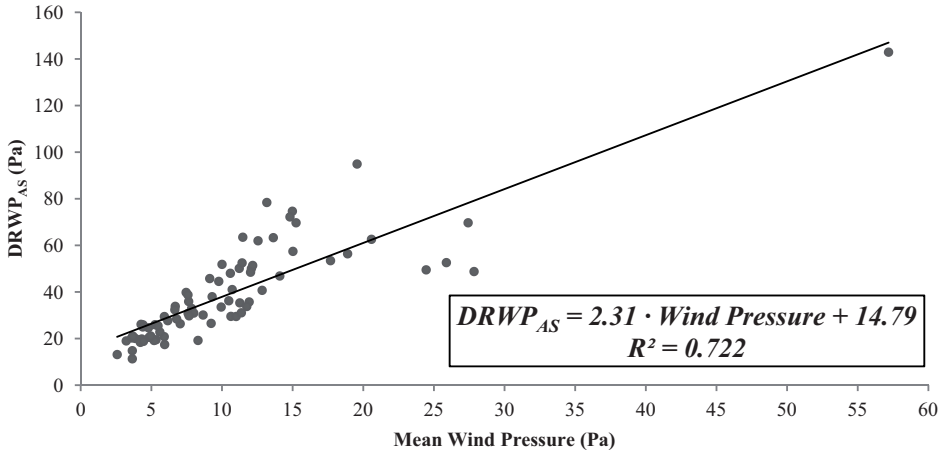

Fig. 4. Best-fit linear relationship between $DRWP_{AS}$ and mean wind pressure in a daily interval.

Figure 5

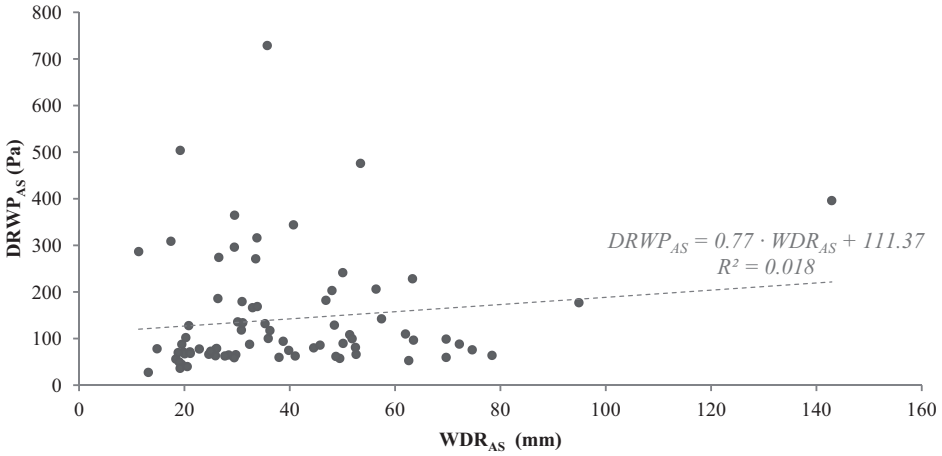

Fig. 5. Convergence between WDR_{AS} and $DRWP_{AS}$ in 80 Spanish locations.

Figure 6

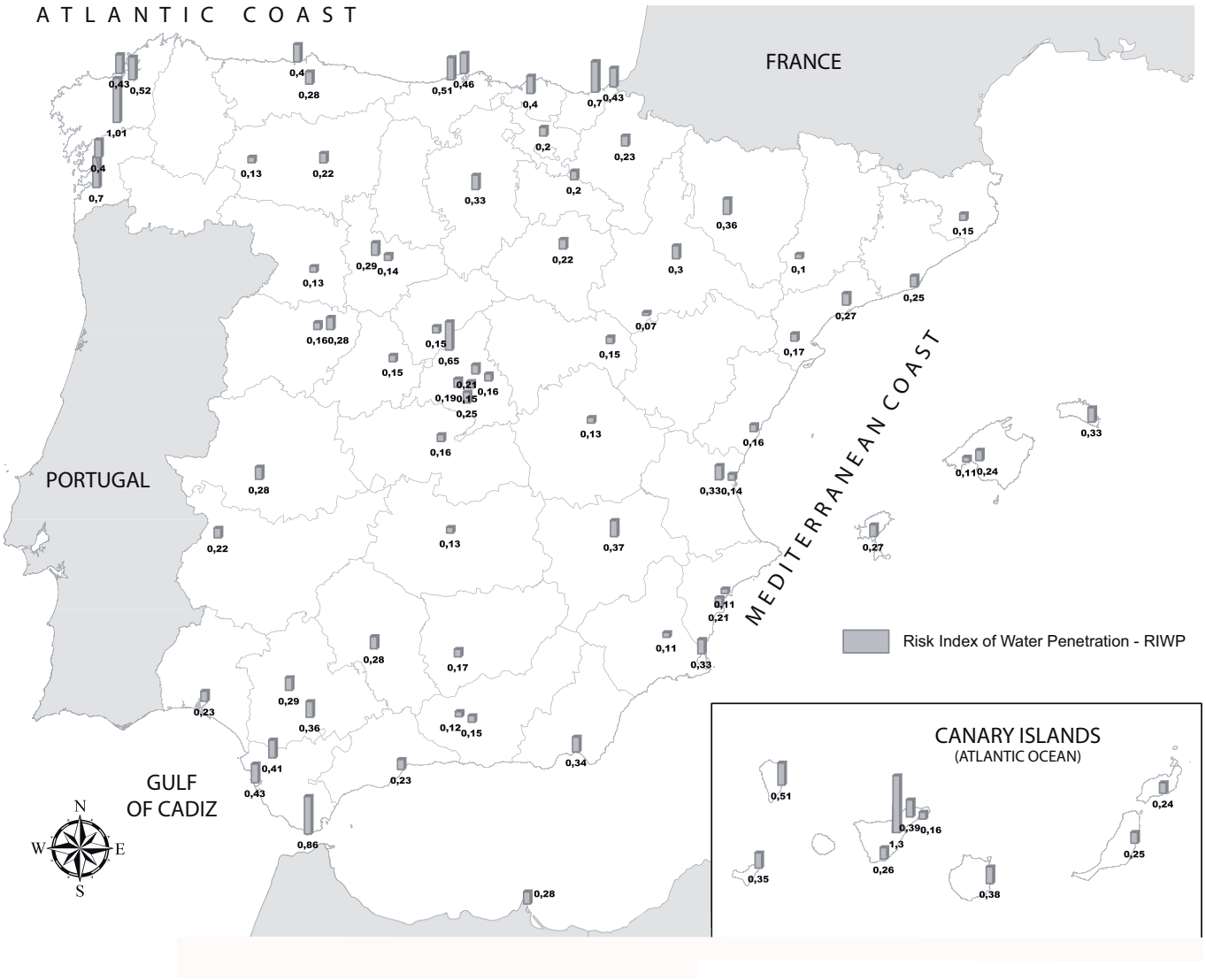

Fig. 6. Risk index of water penetration associated with absolute spells and 3-year return period in Spain.

Figure 7

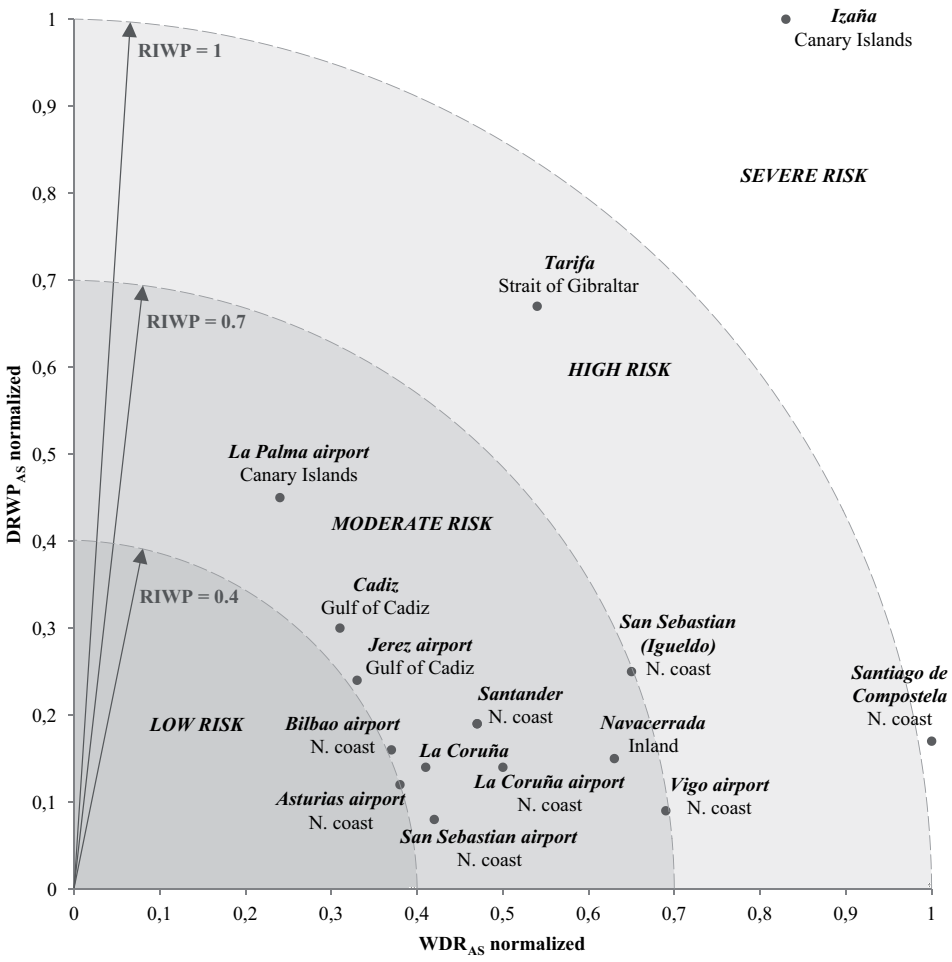

Fig. 7. Viable classification scheme for locations based on the equivalence of both exposure parameters. *Only sites with radii that define a potential to present problems related to water penetration greater than 0.4 are shown.*